nature cell biology

Reprogramming of the tumour microenvironment by stromal PTEN-regulated miR-320

A. Bronisz[1,2], J. Godlewski[3], J. A. Wallace[2], A.S. Merchant[2], M.O. Nowicki[3], H. Mathsyaraja[2], R. Srinivasan[2], A. J. Trimboli[4,5], C. K. Martin[2], F. Li[2,4], L. Yu[6], S. A. Fernandez[6], T. Pécot[4,5,7], T. J. Rosol[8], S. Cory[9,10], M. Hallett[9,10], M. Park[10,11], M. G. Piper[12], C. B. Marsh[12], L. D. Yee[13], R. E. Jimenez[14], G. Nuovo[15], S. E. Lawler[3], E. A. Chiocca[3], G. Leone[1,4,5,16] and M. C. Ostrowski[1,2,16]

PTEN (Phosphatase and tensin homolog deleted on chromosome 10) expression in stromal fibroblasts suppresses epithelial mammary tumours, but the underlying molecular mechanisms remain unknown. Using proteomic and expression profiling, we show that *Pten* loss from mammary stromal fibroblasts activates an oncogenic secretome that orchestrates the transcriptional reprogramming of other cell types in the microenvironment. Downregulation of miR-320 and upregulation of one of its direct targets, ETS2 (v-ets erythroblastosis virus E26 oncogene homolog 2) are critical events in *Pten*-deleted stromal fibroblasts responsible for inducing this oncogenic secretome, which in turn promotes tumour angiogenesis and tumour-cell invasion. Expression of the *Pten*–miR-320–*Ets2*-regulated secretome distinguished human normal breast stroma from tumour stroma and robustly correlated with recurrence in breast cancer patients. This work reveals miR-320 as a critical component of the *Pten* tumour-suppressor axis that acts in stromal fibroblasts to reprogramme the tumour microenvironment and curtail tumour progression.

Stromal cells, including fibroblasts, endothelial cells and immune cells, collaborate with tumour cells to promote tumour proliferation, invasion and metastasis to distant sites. Fibroblasts are particularly important because they coordinate critical interactions between the various stromal and tumour cells by modulating the composition and function of the extracellular matrix. While normal fibroblasts prevent tumour growth and invasiveness, tumour-associated fibroblasts become reprogrammed by unknown mechanisms to co-evolve with epithelial tumour cells and provide an environment conducive for tumour initiation and progression[1–5]. Recently, we showed that genetic inactivation of *Pten* in mammary stromal fibroblasts of mice accelerates the initiation, progression and malignant transformation of mammary epithelial tumours and that this depends on the activation of the transcription factor ETS2 (ref. 6). Importantly, this work demonstrated that decreased PTEN protein levels were frequently observed in the stroma of human invasive-breast-cancer patients and were inversely correlated with the stromal expression of activated phosphorylated v-akt murine thymoma viral oncoprotein homolog 1 (AKT, also known as AKT1) and ETS2. In this report we show that *Pten* loss reprogrammes messenger RNA and microRNA (miR) expression profiles in normal mammary stromal fibroblasts to elicit a tumour-associated fibroblast phenotype and the reprogramming of gene expression in the entire mammary-gland microenvironment. While there is extensive evidence supporting a role for miRs in tumour cells[7,8], little is known about their regulation in stromal fibroblasts and whether they participate in the communication between the different cellular compartments of the

[1]Tumor Microenvironment Program, Comprehensive Cancer Center, The Ohio State University, Columbus, Ohio 43210, USA. [2]Department of Molecular and Cellular Biochemistry, College of Medicine, The Ohio State University, Columbus, Ohio 43210, USA. [3]Dardinger Laboratory for Neuro-oncology and Neurosciences, Department of Neurological Surgery, The Ohio State University Medical Center and James Comprehensive Cancer Center, Columbus, Ohio 43210, USA. [4]Department of Molecular Genetics, College of Biological Sciences, Comprehensive Cancer Center, Ohio State University, Columbus, Ohio 43210, USA. [5]Department of Molecular Virology, Immunology and Medical Genetics, Ohio State University, Columbus, Ohio 43210, USA. [6]Center for Biostatistics, Office of Health Sciences, The Ohio State University, Columbus, Ohio 43210, USA. [7]The Ohio State University Computer Science and Engineering, The Ohio State University Biomedical Informatics, The Ohio State University, Columbus, Ohio 43210, USA. [8]Department of Veterinary Clinical Sciences, College of Veterinary Medicine, The Ohio State University, Columbus, Ohio 43210, USA. [9]McGill Centre for Bioinformatics, McGill University, Montreal, Quebec, H3A0B1, Canada. [10]Department of Biochemistry, Rosalind and Morris Goodman Cancer Center University, Montreal, Quebec, H3A0B, Canada. [11]Department of Oncology, McGill University, Quebec, H3A 1A1, Canada. [12]Division of Pulmonary, Allergy, Critical Care, and Sleep Medicine, Department of Internal Medicine, Dorothy M. Davis Heart and Lung Research Institute, The Ohio State University, Columbus, Ohio 43210, USA. [13]Department of Surgery, School of Medicine, The Ohio State University, Columbus, Ohio 43210, USA. [14]Department of Laboratory Medicine and Pathology, Mayo Clinic, Rochester, Minnesota 55905, USA. [15]Department of Pathology, The Ohio State University Medical Center and James Comprehensive Cancer Center, Columbus, Ohio 43210, USA.
[16]Correspondence should be addressed to G.L. or M.C.O. (e-mail: gustavo.leone@osumc.edu or michael.ostrowski@osumc.edu)

Received 10 January 2011; accepted 7 November 2011; published online 18 December 2011; DOI: 10.1038/ncb2396

tumour microenvironment. We show that miR-320 is a critical target of PTEN in stromal fibroblasts that directly controls ETS2 expression and instructs the tumour microenvironment to suppress many of the aggressive phenotypes associated with advanced stages of breast cancer, including tumour-cell invasiveness and increased angiogenic networks.

RESULTS

Pten loss in stromal fibroblasts reprogrammes gene expression in the mammary-gland microenvironment

To explore the mechanism of how PTEN-mediated signalling in stromal fibroblasts elicits tumour suppression, we compared expression of miRs in mouse mammary fibroblasts (MMFs) containing or lacking *Pten*. The *Fsp–cre* transgene and a conditional allele of *Pten* previously established in our laboratory were used to carry out fibroblast-specific deletion of *Pten* in mammary glands of mice (*Fsp–cre*; $Pten^{loxP/loxP}$; ref. 9). Of 400 miRs profiled, ten miRs conserved between mouse and human genomes were significantly downregulated at least twofold in *Pten*-deleted MMFs (Supplementary Table S1). Quantitative real-time PCR (qrtPCR) confirmed reduced expression of nine of the ten relevant miRs in *Pten*-null fibroblasts (Fig. 1a and Supplementary Table S1). Together, these observations indicate that *Pten* loss influences mRNA (ref. 6) and miR profiles in mammary stromal fibroblasts.

We then entertained the possibility that the specific ablation of *Pten* in MMFs could lead to the reprogramming of gene expression in other cell compartments of the mammary gland. Analysis of mRNA expression profiles derived from epithelial and endothelial cells purified from $Pten^{loxP/loxP}$ and *Fsp–cre*; $Pten^{loxP/loxP}$ mammary glands revealed distinct sets of genes that were differentially expressed dependent on the status of *Pten* in mammary fibroblasts (Fig. 1b and Supplementary Fig. S1a).

miR-320 in fibroblasts suppresses tumour-cell growth *in vivo*

Because miRs impact wide networks of gene expression[10], we focused on miRs in mammary stromal fibroblasts that could potentially function to communicate *Pten* signalling to the other cells in the microenvironment. We selected miR-320 for further analysis because it was the only miR of the nine conserved murine miRs to be reported to be downregulated in human breast cancer[11–15] and because relatively little is known about its function. In four pairs of independently isolated MMF populations, miR-320 expression was significantly reduced when *Pten* was ablated and was inversely correlated with expression of the critical PTEN target ETS2 (Supplementary Fig. S1b). To test whether decreased miR-320 expression had any functional consequence on the behaviour of mammary epithelial tumour cells, we ectopically expressed miR-320 in *Pten*-null MMFs (Supplementary Fig. S2d) and evaluated their capacity to support epithelial tumour-cell growth in xenograft assays. A mouse mammary epithelial tumour-cell line expressing a variant of the polyoma virus middle T-antigen gene (DB7; ref. 16) was tagged with dsRed and co-injected with enhanced green fluorescent protein (GFP)-tagged MMFs into immunocompromised mice. When compared with the co-injection of $Pten^{+/+}$ MMFs, the co-injection of $Pten^{-/-}$ MMFs increased tumour growth fourfold, whereas restoration of miR-320 expression in the $Pten^{-/-}$ MMFs significantly reduced tumour growth (Fig. 1c). Differences in tumour size were due almost exclusively to an increase in the epithelial tumour-cell compartment, as determined by the ratio of dsRed tumour cells to enhanced GFP MMFs visualized by confocal microscopy (Supplementary Fig. S2a). Importantly, tumours derived from DB7 cells co-injected with $Pten^{-/-}$ MMFs expressing miR-320 were less invasive and had diminished vasculature when compared with tumours from DB7 cells co-injected with $Pten^{-/-}$ MMFs (Supplementary Fig. S2b,c).

To capture the direct effects of fibroblasts on the tumorigenicity of epithelial cells without the potential confounding effects of infiltrating host stromal cells, we transiently expressed miR-320 or anti-miR-320 in MMFs and analysed the consequences on DB7 tumour cells at an earlier time in tumour development. These experiments had two complementary arms. First, co-injection of DB7 cells with $Pten^{-/-}$ MMFs was compared with the co-injection of DB7 with $Pten^{-/-}$ MMFs re-expressing miR-320. In this set of experiments, tumour-cell proliferation, measured by 5-bromodeoxyuridine (BrdU) incorporation, decreased by approximately 30% with miR-320 re-expression in $Pten^{-/-}$ MMFs (Fig. 1d, top panels). The formation of new blood vessels in these tumours, as measured by CD31 (platelet/endothelial cell adhesion molecule, also known as PECAM1) immunostaining, was also significantly decreased by the re-expression of miR-320 in $Pten^{-/-}$ MMFs (Fig. 1e, top panels). In the complementary second set of experiments, DB7 cells were co-injected with $Pten^{+/+}$ MMFs or with $Pten^{+/+}$ MMFs knocked down for endogenous miR-320 (through anti-miR, see Supplementary Fig. S2e). In these experiments, tumour-cell proliferation increased by approximately 25% with knockdown of miR-320 in $Pten^{+/+}$ MMFs (Fig. 1d, bottom panels). Similarly, the formation of new blood vessels was markedly increased by anti-miR-320 knockdown (Fig. 1e, bottom panels). Taken together, these results uncover a cell-non-autonomous tumour-suppressor role for miR-320 in stromal fibroblasts.

miR-320 and PTEN expression are correlated in human breast cancer stroma but not in the tumour

We then examined stromal and epithelial expression of miR-320 in a panel of human invasive breast carcinoma and matched normal samples from 126 patients by *in situ* hybridization[17]. The human genome contains eight annotated *MIR320* genes that encode five mature miR variants; the mouse has an orthologue for only one of these, miR-320a. We used the *Mir320a* sequence to design the locked oligonucleotide probe used for this analysis; however, all five variant miRs would probably be detected with the hybridization conditions used. Robust miR-320 expression was detected in the epithelial and stromal cell compartments of normal breast tissue but was consistently reduced in both cell compartments of invasive carcinoma samples (multispectral blue-channel images and quantification in Fig. 2a, light microscope images in Supplementary Fig. S3a). Some nuclear staining for miR-320 was also evident. This nuclear staining could be explained either by probe hybridization to nuclear pre-miR forms or by nuclear re-localization of the mature miR (refs 18–22).

Multispectral imaging of samples stained for both PTEN and miR-320 demonstrated that their expression could be co-localized in the tumour stroma (Fig. 2b and Supplementary Fig. S3b). When the staining of PTEN and miR-320 was scored, a significant positive correlation between PTEN and miR-320 expression in the tumour stroma was revealed (Spearman rho = 0.24, $P = 0.004$, Supplementary Table S2). In contrast, there was no significant correlation between

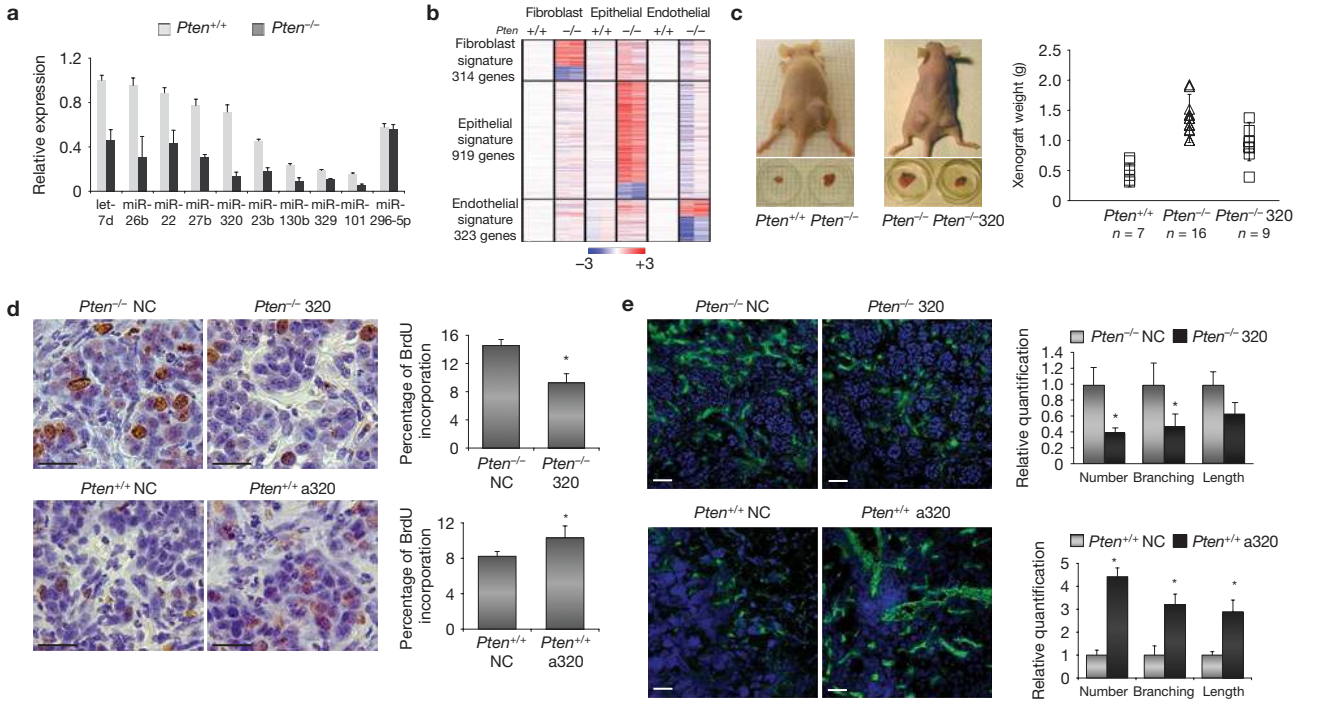

Figure 1 miR-320 is a PTEN target in fibroblasts that suppresses tumour growth. (**a**) Expression of selected microRNAs was validated by qrtPCR in three sets of primary *Pten*$^{+/+}$ or *Pten*$^{-/-}$ MMFs. Relative miR expression level (normalized to 18S ribosomal RNA) is shown as mean ± s.d. miR-296-5p is an example of a miR whose expression did not change. $n = 4$. (**b**) Gene profiling was carried out ($n = 2$) on three types of cell from mammary glands with *Pten*$^{LoxP/LoxP}$ (*Pten*$^{+/+}$) or *Fsp–cre*; *Pten*$^{LoxP/LoxP}$ (*Pten*$^{-/-}$) as indicated. The heat map shows the gene signature with 314 genes changed in fibroblasts, 919 genes changed in epithelial cells and 323 genes changed in endothelial cells (>2-fold and $P < 0.05$). (**c**) Representative images of tumours before and after excision from mice injected with DB7 cells admixed with *Pten*$^{+/+}$ ($n = 7$) or *Pten*$^{-/-}$ ($n = 16$) MMFs (left panel), and DB7 cells admixed with *Pten*$^{-/-}$ MMFs or *Pten*$^{-/-}$ cells re-expressing miR-320 ($n = 9$) (right panel). Tumour weights were quantified after four weeks, and the data are expressed as mean ± s.d. All three groups were tested by analysis of variance and subsequent adjusted pairwise comparisons were carried out. These comparisons were significant: *Pten*$^{+/+}$ versus *Pten*$^{-/-}$ MMFs, $P = 5.58 \times 10^{-6}$; *Pten*$^{+/+}$ versus *Pten*$^{-/-}$ miR-320 MMFs, $P = 0.022215$; *Pten*$^{-/-}$ versus *Pten*$^{-/-}$ miR-320 MMFs, $P = 0.007976$. (**d**) Epithelial tumour-cell proliferation measured by BrdU incorporation in xenografts composed of DB7 cells admixed with *Pten*$^{-/-}$ or *Pten*$^{+/+}$ MMFs transfected with either negative control (NC), miR-320 (320, upper right panel) or anti-miR-320 (a320, lower right panel); $n = 4$ for each group. The epithelial/fibroblast composites were collected five days after subcutaneous growth in mice. BrdU injection was carried out 3 h before collecting the tissue. Scale bars, 25 μm. Data are expressed as mean ± s.d. $^*P < 0.05$. (**e**) Angiogenesis determined using CD31 staining to detect blood vessels in nascent tumours composed of DB7 cells and the same *Pten*$^{-/-}$ or *Pten*$^{+/+}$ MMFs transfected with negative control (NC), miR-320 (320, upper panels) or anti-miR-320 (a320, lower panels), as above; $n = 4$ for each group. The epithelial/fibroblast mixtures were grown for five days subcutaneously in mice. Representative micrographs showing merged images are shown (green, CD31; blue, 4,6-diamidino-2-phenylindole, DAPI). Scale bars, 50 μm. Data are expressed as mean ± s.d. $^*P < 0.05$.

PTEN and miR-320 in the epithelial tumour-cell compartment of the same tissue microarray (TMA) samples (Spearman rho = 0.093, $P = 0.268$). Interestingly, a significant inverse correlation was found between PTEN expression in the tumour and tumour stroma, whereas a strong positive correlation was found between miR-320 expression in the tumour and tumour stroma (Supplementary Table S2), suggesting that downregulation of miR-320 in the stroma and tumour compartments may be mediated through distinct mechanisms.

Given the established relationship between PTEN function and ETS2 (ref. 6), we used these tissue arrays to examine the phosphorylation status of Thr 72 in ETS2 (P-ETS2^{T72}), which corresponds to its active state as a transcriptional activator. This analysis revealed that P-ETS2^{T72} levels inversely correlated with miR-320 levels in breast carcinoma samples (Spearman correlation coefficient −0.166, $P = 0.04$, Supplementary Table S2). The correlative human data raised the possibility of a functional connection between PTEN and miR-320 in blocking the function of ETS2 in stromal fibroblasts in a way that might bias the mammary gland microenvironment towards tumour suppression.

miR-320 in stromal fibroblasts suppresses tumour-cell and endothelial-cell proliferation and invasion *in vitro*

Increased proliferation and migration of epithelial cells with concurrent epithelial–mesenchymal transition are hallmarks of malignant tumour growth[23,24]. Stromal fibroblasts are known to produce factors that signal to other cell types in the tumour microenvironment[25]. To determine whether miR-320 in stromal fibroblasts influences the invasiveness of epithelial tumour cells, we developed a three-dimensional sphere invasion assay to monitor and quantify the migration of a non-invasive breast cancer tumour-cell line (DB7). As monitored by microscopy, DB7 epithelial tumour cells embedded in a type I collagen matrix did not migrate to any appreciable extent when incubated with either fresh media or conditioned media derived from wild-type MMFs (Fig. 3a, left and middle panels). In contrast, migration was markedly increased when DB7 cells were incubated with conditioned medium from *Pten*-null MMFs (Fig. 3a, right panel). Interestingly, conditioned media from *Pten*-null MMFs elicited morphological changes in DB7 cells that resembled epithelial–mesenchymal transition (Fig. 3a, magnified insets). Using this invasion assay, we could show that

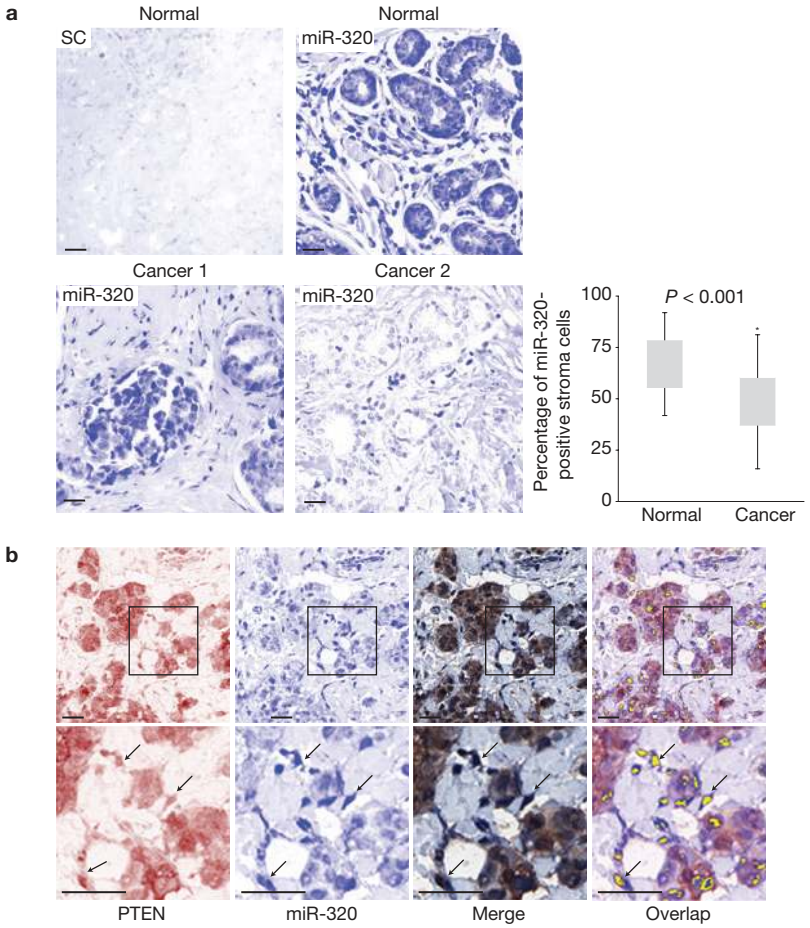

Figure 2 miR-320 and PTEN are co-expressed in human tumour stroma. (**a**) Representative images of miR-320 *in situ* hybridization (ISH) staining in paraffin-imbedded, human normal (control) and breast cancer tissue; scrambled control (SC) was carried out on adjacent normal breast tissue. Images were captured with the Nuance multispectral system (blue channel shown). Scale bars, 50 μm. The percentage of positive cells per random field was determined in normal and carcinoma TMA sections from 126 matched patient samples (Methods); results are shown as mean ± s.d. on the graph. $P = 1.76 \times 10^{-15}$. (**b**) Representative multispectral images of human breast carcinoma TMA samples stained for both miR-320 (ISH staining, blue) and PTEN (IHC, red). Upper panels, low magnification; lower panels, high magnification. Scale bars, 50 μm. Co-localization of miR-320 and PTEN signals determined from the merged image was converted to fluorescent (yellow) signal using the Nuance multispectral system and is indicated by the arrows.

re-expression of miR-320 in *Pten*-null MMFs attenuated the migration capacity of DB7 cells and also restored their typical cuboidal epithelial morphology (Fig. 3b). BrdU-incorporation assays demonstrated that conditioned media from *Pten*-null MMFs overexpressing miR-320 eventually led to a modest but consistent decrease in the proliferation of DB7 cells (Fig. 3c).

Because co-injection of DB7 cells with MMFs lacking *Pten* or miR-320 resulted in highly vascular tumours, we examined whether miR-320 in MMFs might directly influence the behaviour of endothelial cells using three-dimensional tube formation assays. Conditioned media from *Pten*-null MMFs stimulated the invasion of endothelial cells into matrigel and enhanced their arrangement into branched, tube-like structures, whereas conditioned media from miR-320-expressing *Pten*-null MMFs mitigated these effects (Fig. 3d). Moreover, conditioned media from *Pten*-null MMFs overexpressing miR-320 led to a decrease in the proliferation of endothelial cells when compared with control (Fig. 3e). Thus, we conclude that miR-320 in stromal fibroblasts profoundly influences the behaviour of other cell types in the tumour microenvironment through the action of secreted factors.

Stromal miR-320 regulates a tumour-specific secretome

We used a proteomic approach to identify the miR-320-regulated factors secreted by fibroblasts that modulate tumour- and endothelial-cell function. Mass spectrometry analysis of unfractionated, conditioned media from *Pten*-null MMFs, expressing either miR-320 or a negative control miR, identified 51 secreted proteins that were differentially represented, with 32 unique proteins present in the conditioned media from control *Pten*-null MMFs and 19 proteins unique to the conditioned media from miR-320-expressing *Pten*-null MMFs (Supplementary Fig. S4a,b and Table S3).

Western blot analysis on a subset of these proteins confirmed their differential secretion and also identified quantitative changes in the level of three more secreted proteins that were not reproducibly detected by mass spectrometry, giving rise to a miR-320-responsive secretome profile of 54 factors (Fig. 4a and Supplementary Fig. 7a and Table S3). Three main groups of secreted factors were identified in the 54-factor secretome. In the first group, secreted factors such as matrix metallopeptidase 9, matrix metallopeptidase 2, bone morphogenetic protein 1, lysyl oxidase-like 2 (MMP9, MMP2, BMP1, LOXL2 respectively) and elastin

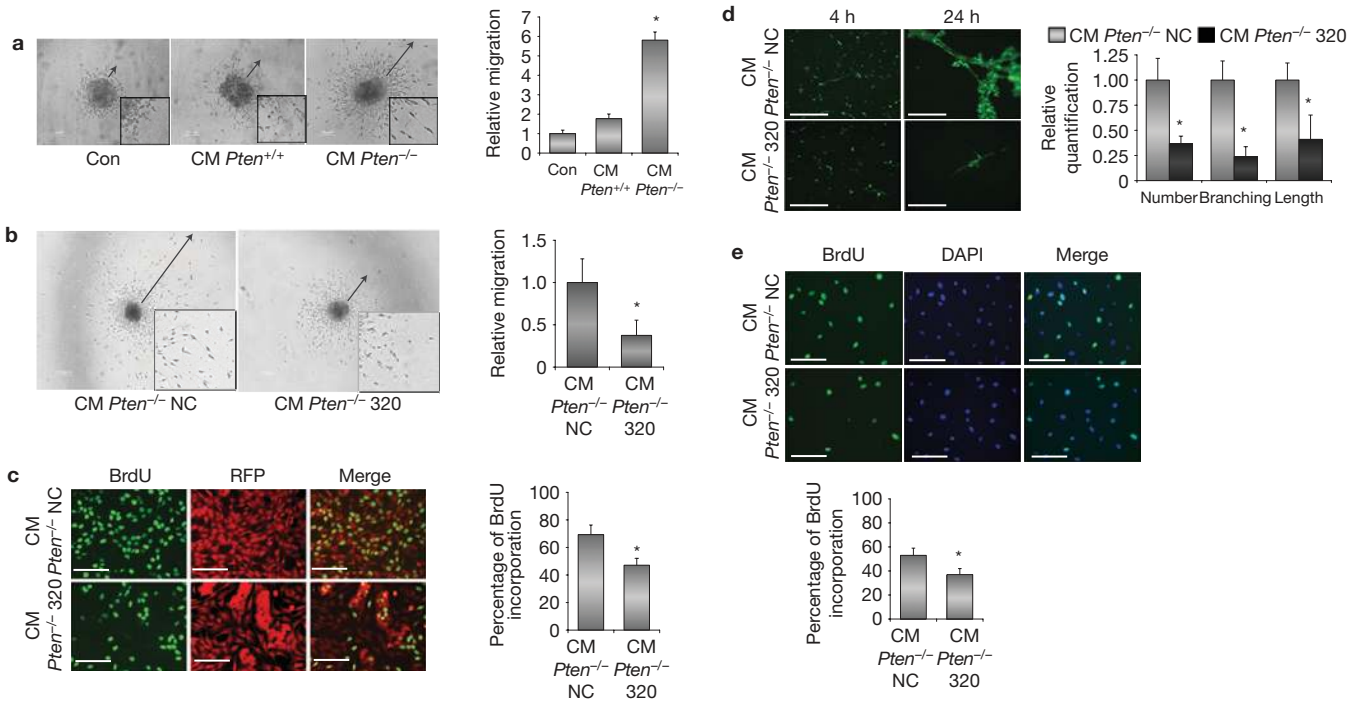

Figure 3 *Pten* and miR-320 in fibroblasts control tumour-cell migration and growth. (**a**) Left: representative images of DB7 mammospheres in the presence of DMEM/fetal bovine serum medium (Con) ($n=6$) or conditioned medium (CM) produced by either $Pten^{+/+}$ ($n=4$) or $Pten^{-/-}$ ($n=6$) MMFs. Scale bars, 100 μm. The insets in all panels are magnified ×2.5. Right: quantification of migratory zones indicated by arrows expressed as mean area of migration ±s.d., $^{*}P<0.01$. (**b**) Left: representative images of DB7 mammospheres in the presence of conditioned medium from $Pten^{-/-}$ MMFs expressing miR negative control ($Pten^{-/-}$ NC) ($n=12$) or miR-320 precursor ($Pten^{-/-}$ 320) ($n=12$). Scale bars, 200 μm. Right: quantification of migratory zones indicated by arrows expressed as mean area of migration ±s.d., $^{*}P<0.01$. (**c**) Left: representative images of BrdU incorporation in DB7 cells in the presence of conditioned medium from MMFs expressing miR negative control ($Pten^{-/-}$ NC) ($n=4$) or with miR-320 precursors ($Pten^{-/-}$320) (n=4). RFP, red fluorescent protein. Scale bars, 100 μm. Right: quantification of BrdU incorporation. Data expressed as mean±s.d., $^{*}P<0.01$. (**d**) Left: representative images of tube-like formation of endothelial cells grown on Matrigel in the presence of conditioned medium from MMFs expressing miR negative control ($Pten^{-/-}$ NC) ($n=3$) or with miR-320 precursor ($Pten^{-/-}$320) ($n=3$). Right: quantification of tube formation expressed as mean±s.d., $^{*}P<0.01$. Scale bars, 50 μm. (**e**) Top: representative images of BrdU incorporation by endothelial cells in the presence of conditioned medium from MMFs expressing miR negative control ($Pten^{-/-}$ NC) ($n=3$) or with miR-320 precursors ($Pten^{-/-}$320) ($n=3$). Scale bars, 100 μm. Bottom: quantification of BrdU incorporation. Data expressed as mean±s.d., $^{*}P<0.01$.

microfibril interfacer 2 (EMILIN2) were increased in $Pten^{-/-}$ MMFs. Re-introduction of miR-320 into the cells resulted in decreased expression of these secreted factors to near-normal levels (Fig. 4a, group I), suggesting that they may represent direct targets of miR-320. In the second group, secreted factors such as thrombospondin 1 (THBS1) and secreted frizzled-related protein 1 (SFRP1) were downregulated in $Pten^{-/-}$ MMFs and re-introduction of miR-320 restored their expression (Fig. 4a, group II), and thus probably represent indirect targets of miR-320. Importantly, overexpression of anti-miR-320 (Supplementary Fig. S2e) led to an increase in the secretion of MMP9, MMP2, LOXL2 and EMILIN2 and a decrease in the secretion of THBS1 and SFRP1 (Fig. 4a, groups I and II). The third group of factors, represented by cathepsin B (CTSB), was markedly increased in $Pten^{-/-}$ MMFs but remained unaffected by miR-320 re-expression (Fig. 4a, group III). Conditioned media had no effect on the expression of the miR-320 targets in DB7 cells (Supplementary Fig. S4c).

Two members of the *Pten*-regulated secretome were selected for further analysis, MMP9 and EMILIN2, which are thought to be involved in the control of epithelial-cell migration[26] and angiogenesis[27]. Blocking MMP9 expression from stromal fibroblasts either by *Mmp9*-specific short interfering RNA (siRNA) or by treating conditioned media with an MMP9-specific antibody blunted the ability of conditioned media derived from *Pten*-null MMFs to promote the migration of DB7 cells (Fig. 4b,c). Similarly, blocking EMILIN2 expression by either *Emilin2*-specific siRNA or antibody reduced the ability of *Pten*-null MMF conditioned media to stimulate endothelial cell proliferation (Fig. 4d,e). Thus, these results indicate that miR-320 regulates a fibroblast secretome required for remodelling of the extracellular matrix and vascular network.

Ets2 is a direct target of miR-320

Of the stromal-secreted proteins identified, only seven were predicted by miR/target-recognition software to represent direct targets of miR-320 (Supplementary Table S3), indicating that regulation of this secretome may predominantly be an indirect consequence of miR-320 downregulation. Interestingly, *Ets2* was among the genes predicted to be directly regulated by miR-320 (Supplementary Fig. S5a). Moreover, promoter/enhancer sequences in 20 genes of the 54-factor secretome (37%) contain ETS2-binding elements that are conserved across species[28–33] (Supplementary Table S4), including *Mmp9*, which is a known *bona fide* transcriptional target of ETS2 (ref. 6). Based on the observed correlative relationship between PTEN, ETS2 and miR-320 expression in both MMFs and breast cancer samples, and the above *in silico* predictions, we entertained the possibility that ETS2 may be

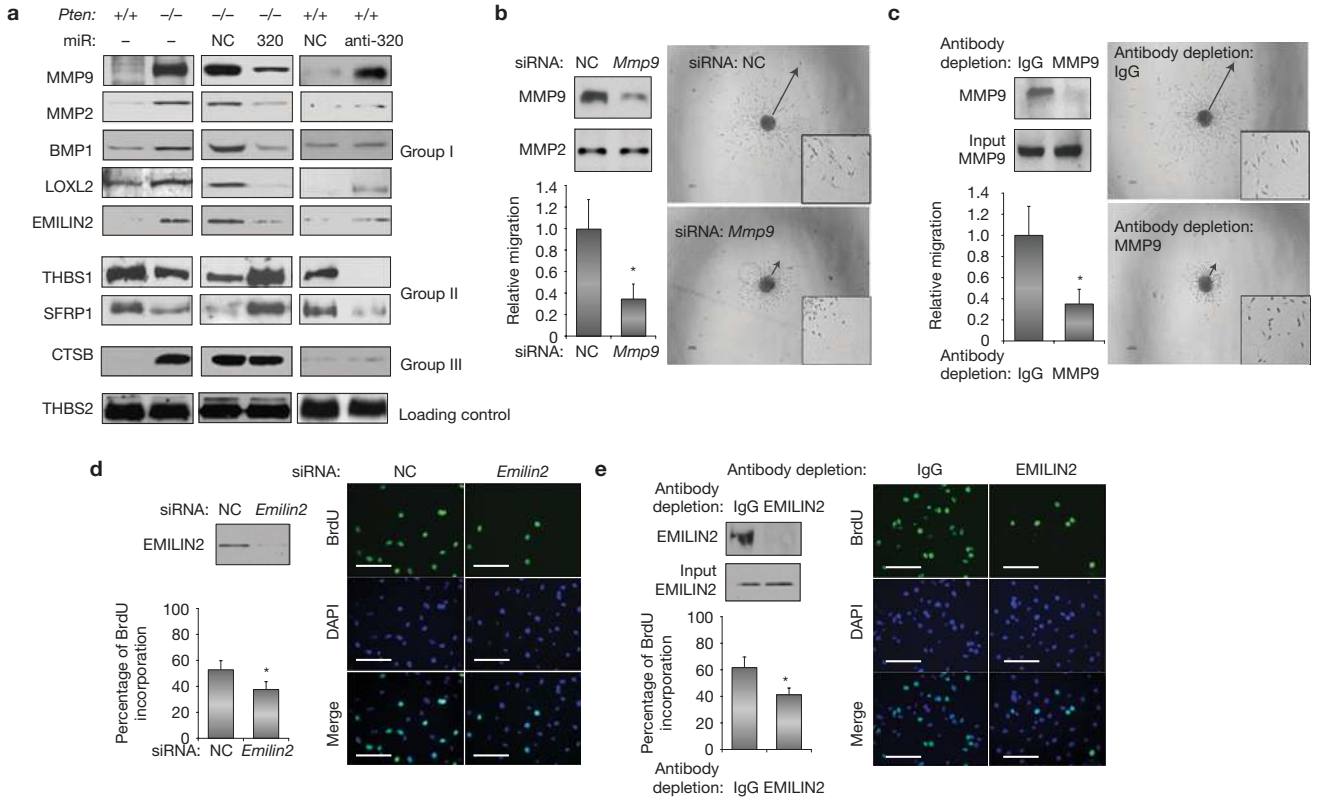

Figure 4 miR-320 regulates the secretome of MMFs. (**a**) *Pten*$^{+/+}$ and *Pten*$^{-/-}$ MMFs were left untreated (lanes 1 and 2) or were transiently transfected with miR negative control (NC), miR-320 precursors (320) or anti-miR-320 precursor (anti-320), respectively. Conditioned media were examined by Western blotting with antibodies against the indicated proteins; thrombospondin 2 (THBS2) serves as an internal control. (**b**) Representative images of DB7 mammospheres in the presence of conditioned medium from *Pten*$^{-/-}$ MMFs expressing siRNA negative control (NC) ($n=4$) or siRNA against *Mmp9* ($n=4$). MMP9 downregulation was verified by Western blot using MMP9 antibody. MMP2 was used as a loading control. Scale bars, 200 μm. The insets in all panels are magnified ×2.5. Quantification of migratory zones (indicated by arrows) expressed as mean area of migration ±s.d., $^*P<0.01$ (bar graphs). (**c**) Representative images of DB7 mammospheres in the presence of conditioned medium from *Pten*$^{-/-}$ MMFs precleared with IgG ($n=4$) or IgG precoupled with α-MMP9 ($n=4$). Western blots using MMP9 antibody in precleared and input control samples were carried out as a control. Scale bars, 200 μm. The insets in all panels are magnified ×2.5. Quantification of migratory zones (indicated by arrows) expressed as mean area of migration ±s.d., $^*P<0.01$ (bar graphs). (**d**) Representative images of BrdU incorporation in endothelial cells in the presence of conditioned medium from *Pten*$^{-/-}$ MMFs expressing siRNA negative control (NC) ($n=3$) or siRNA against *Emilin2* ($n=3$). EMILIN2 downregulation was verified by Western blot using EMILIN2 antibody. Scale bars, 100 μm. Quantification of BrdU incorporation expressed as mean ± s.d., $^*P<0.01$. (**e**) Representative images of BrdU incorporation in endothelial cells in the presence of conditioned medium from *Pten*$^{-/-}$ MMFs precleared with IgG ($n=3$) or IgG precoupled with α-EMILIN2 ($n=4$). Western blots using EMILIN2 antibody in precleared and input control samples were carried out as a control. Scale bars, 100 μm. Quantification of BrdU incorporation expressed as mean ± s.d., $^*P<0.01$. Full-length blots are presented in Supplementary Fig. S7a.

acting downstream of miR-320 to regulate the expression of a large fraction of the 54-factor secretome.

Consistent with this hypothesis, reintroduction of miR-320 in *Pten*-null MMFs led to a decrease in ETS2 protein levels, and, conversely, overexpression of the anti-miR-320 in wild-type fibroblasts increased ETS2 protein to levels found in *Pten*$^{-/-}$ MMFs (Fig. 5a and Supplementary Fig. S7b); no significant effects on the signalling pathways of AKT, mitogen-activated protein kinase 8/9 (JNK1/2; also known as MAPK8/9) and Eph receptor B2 (ERK; also known as EPHB2), known to be upstream activators of ETS2 (ref. 6), were observed on manipulation of miR-320 levels (Supplementary Fig. S5b). To test if miR-320 directly regulates ETS2, we examined the ectopic expression of an *Ets2* full-length complementary DNA with an authentic 3′ untranslated region (3′UTR) containing the predicted miR-320 target sequences. Co-transfection of miR-320 along with this full-length *Ets2* cDNA vector resulted in a marked decrease in ectopic ETS2 protein levels. Mutation of the predicted miR-320 target sequences in the *Ets2* 3′UTR abolished this effect (Fig. 5b and Supplementary Figs S5c, S7b). Moreover, introduction of the *Ets2* 3′UTR into a luciferase reporter gene was sufficient to modulate reporter expression in response to miR-320 (Supplementary Fig. S5d).

In silico analysis also predicted *Mmp9* and *Emilin2* to be direct targets of miR-320. Employing an experimental strategy similar to that described above, we could show that *Mmp9* and *Emilin2* are directly regulated by miR-320 through their 3′UTR target sequences (Fig. 5c and Supplementary Figs S5c, S7c; luciferase reporter gene assays in Supplementary Fig. S5d). Exogenous introduction of miR-320 into *Pten*-null MMFs also led to decreased *Ets2*, *Mmp9* and *Emilin2* mRNA levels (Supplementary Fig. S5e). These results are consistent with a dual mechanism for the regulation of *Mmp9* expression that involves transcriptional control by ETS2 (ref. 6) and posttranscriptional control by miR-320.

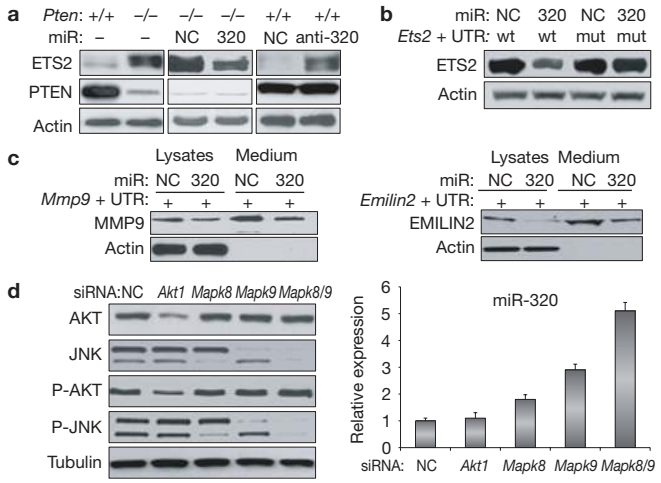

Figure 5 Identification and characterization of *Ets2*, *Mmp9* and *Emilin2* as *bona fide* targets of miR-320. (**a**) $Pten^{+/+}$ and $Pten^{-/-}$ MMFs were left untreated (lanes 1 and 2) or were transiently transfected with miR negative control (NC), miR-320 precursors (320) or anti-miR-320 (anti-320), respectively. Nuclear extracts were blotted with anti-ETS2 antibody or anti-PTEN antibody; anti-β-actin antibody was used as a loading control. (**b**) COS7 cells were transfected with full-length cDNA (5′-UTR–open reading frame–3′-UTR) of *Ets2* (*Ets2*+UTR) wild type (wt) or mutated in miR-320 seeding region (mut) expression vector and co-transfected with either miR negative control (NC) or miR-320 precursors (320). Cell lysates or conditioned medium were blotted with anti-ETS2 antibody; anti-β-actin antibody was used as a loading control. (**c**) COS7 cells were transfected with full-length cDNA (5′-UTR–open reading frame–3′-UTR) of *Mmp9* (*Mmp9*+UTR) (left panel) or *Emilin2* (*Emilin2*+UTR) (right panel) and co-transfected with either miR negative control (NC) or miR-320 precursors (320). Cell lysates or conditioned medium were blotted with anti-MMP9 or anti-EMILIN2 antibody; anti-β-actin antibody was used as a loading control. (**d**) $Pten^{-/-}$ MMFs were transiently transfected either with siRNA negative control (NC) or siRNA against *Akt1*, *Mapk8*/*Jnk1*, *Mapk9*/*Jnk2* or the combination of *Mapk8*/*Jnk1* and *Mapk9*/*Jnk2*. AKT and JNK phosphorylation status was verified by Western blot using anti-phospho-specific antibodies, and compared with total kinase levels using non-discriminating antibodies. Tubulin was used as a loading control. Expression of miR-320 was validated by qrtPCR ($n = 3$). Mean relative miR expression level ±s.d. is shown. Full-length blots are presented in Supplementary Fig. S7b–d.

Loss of *Pten* leads to activation of the phosphatidylinositol 3 (PI3)-kinase/AKT pathway, which is believed to be the pathway responsible for the majority of phenotypes associated with loss of *PTEN* in human tumours[34]. However, *Pten* loss has also been shown to activate further signalling pathways, including AKT-independent activation of the JNK pathway[35,36]. Based on preliminary results using small-molecule inhibitors for PTEN-regulated pathways (data not shown), we focused on AKT1, JNK1/MAPK8 and JNK2/MAPK9 using the more specific approach of siRNA-mediated knockdown (Fig. 5d and Supplementary Fig. S7d). These experiments demonstrated that knockdown of either *Jnk1*/*Mapk8* or *Jnk2*/*Mapk9* in *Pten*-null fibroblasts led to a two- to threefold increase in miR-320 expression, and knockdown of both led to a fivefold increase in miR-320 expression. In contrast, knockdown of *Akt1* had no significant effect on miR-320 expression.

A mouse stromal miR-320 profile predicts human breast cancer patient outcome

To explore the clinical relevance of our findings, we used the mouse-derived 54-secretome profile identified above to query stroma-specific expression profiles of breast cancer patients[37]. Human homologues of the mouse 54-factor secretome profile were differentially expressed in tumour versus adjacent normal stroma[38], leading to a partial segregation of tumour stroma and normal stroma that attained statistical significance (Fig. 6a and Supplementary Table S5). Importantly, the 54-factor secretome profile correlated with clinical outcome based on stromal gene expression in breast cancer patients[37] (Fig. 6b). Given the role of *Ets2* in regulating the expression of a subset of these 54 genes (20/54), we also used this miR-320/*Ets2*-regulated 20-gene subset to query the same stroma-specific expression profiles derived from breast cancer patients. As shown in Fig. 6c, the 20-gene *Ets2* subset differentiated tumour stroma from adjacent normal stroma even more effectively than the complete 54-gene list (Fig. 6c and Supplementary Table S5) and robustly correlated with patient outcome (Fig. 6d). The 54- or the 20-gene secretome profiles, when used to query further expression profiles derived from whole tumours and linked to breast cancer patient outcome data[39], also correlated with patient outcomes (Supplementary Fig. S6a,b).

DISCUSSION

Here, we have identified a *Pten*–miR-320–*Ets2* tumour-suppressor axis in stromal fibroblasts that modulates the intercellular communication within the tumour microenvironment and is responsible for pathological and molecular events observed in malignant human breast cancer. Loss of *Pten* in stromal fibroblasts results in downregulation of miR-320 and the reprogramming of mRNA expression profiles in neighbouring endothelial and epithelial cells of the mammary gland. We show that, by influencing the behaviour of multiple cell types, miR-320 in stromal fibroblasts is a critical *Pten*-regulated determinant for the suppression of epithelial tumours. Despite identifying a critical function for the miR-320–*Ets2* pathway in the stroma, our results do not show that the miR-320–*Ets2* pathway is strictly stromal specific. The pathway could also be active in epithelial tumour cells that have low PTEN expression, although the PTEN immunohistochemistry (IHC) results indicate that in the majority of human breast cancer patients the pathway is unlikely to be active in both cell compartments.

Proteomic analysis of fibroblast-conditioned medium identified a miR-320-regulated tumour-promoting secretome that when activated by loss of *Pten* incites profound changes in endothelial and epithelial cell phenotypes typical of malignant tumours. While some of the mRNAs encoding these secreted factors are targeted by miR-320 directly, for example *Emilin2*, most are regulated indirectly through transcriptional control by ETS2, which is itself an essential direct target of miR-320. Together, these findings expose a miR-320 regulatory switch in normal fibroblasts that operates in a cell-autonomous fashion to inhibit the expression of a tumour-promoting secretome and in a cell-non-autonomous fashion to block expression programmes in other cell types in the microenvironment that together suppress tumour-cell growth and invasiveness. Remarkably, bioinformatic analyses demonstrated that a miR-320 secretome signature could distinguish normal from tumour stroma and could be used to robustly predict outcome in breast cancer patients, underlining the potential clinical impact of the stromal *Pten*–miR-320 regulatory axis on human breast cancer.

In conclusion, our results extend the concept of miR function beyond the tumour cell boundary by defining a complex network

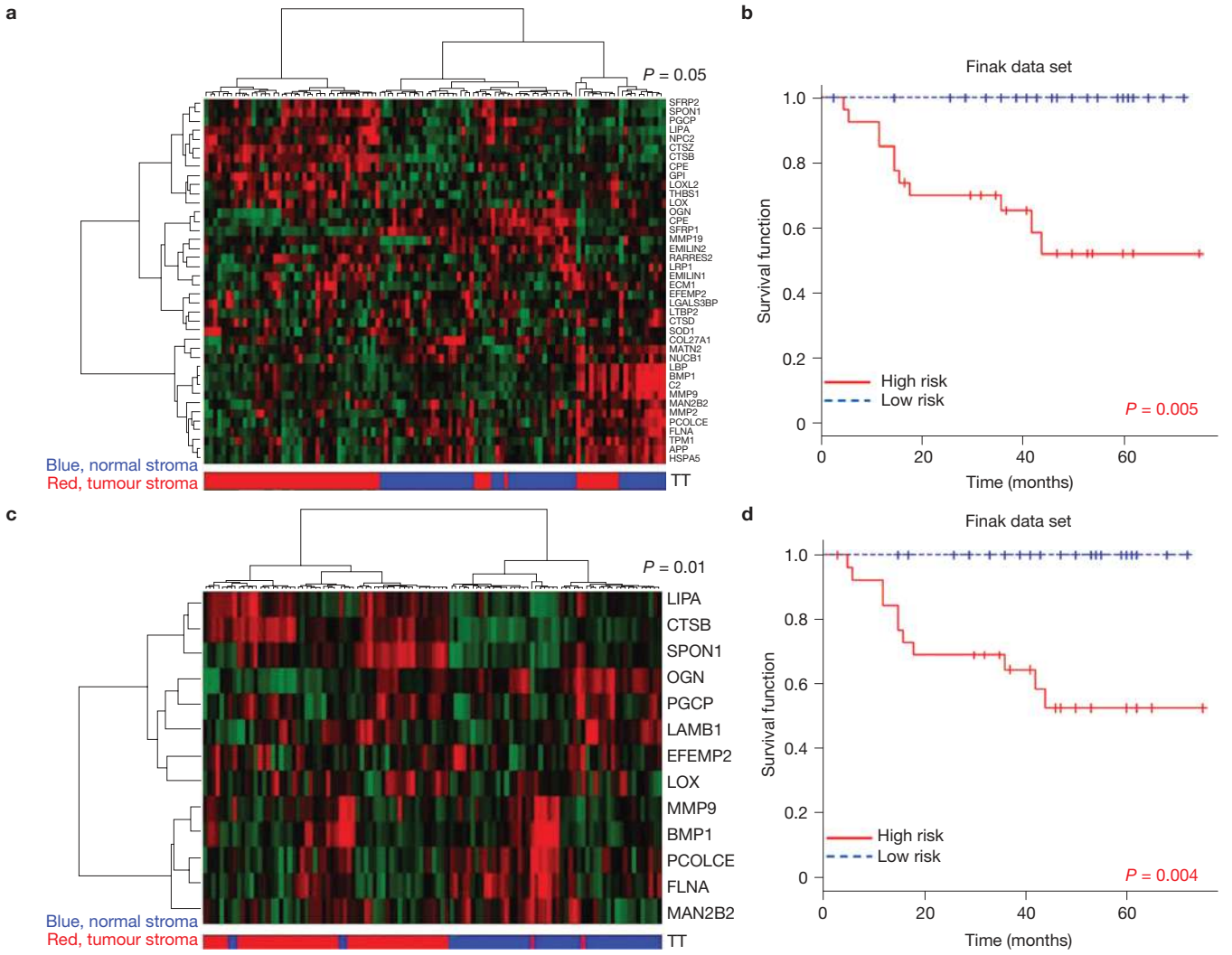

Figure 6 The miR-320 secretome profile separates human breast normal and cancer stroma (tumour type, TT) and predicts patient outcome. (**a**) Heat map showing the differential expression in human tumour versus normal stroma of the 40 human orthologues from the 54-factor mouse secretome that were retrieved from the McGill stromal microarray (GSE4823). The *P* value indicates the ability of the 40-gene signature to partition normal and tumour stroma when compared with 10,000 random permutations (Methods). (**b**) Kaplan–Meier curves of high- and low-risk groups based on expression of the 40-gene secretome signature present in the GSE9014 dataset. Expression of the 40-gene secretome signature correlates with poor patient outcomes. The permutation *P* value of the log-rank test statistic between risk groups is based on 1,000 permutations. (**c**) Heat map showing the differential expression in tumour versus normal stroma of 13 human orthologues from the 20 ETS2-target genes that were retrieved from the McGill breast cancer stroma microarray (GSE4823). The *P* value indicates the ability of the mouse 17-gene signature to partition normal and tumour stroma as above (Methods). (**d**) Kaplan–Meier survival curves of high- and low-risk groups based on expression of the 13-gene ETS2-related secretome signature. Expression of the subset of secretome genes directly regulated by ETS2 (13/20 genes in GSE4823) correlates with poor patient outcome. The permutation *P* value of the log-rank test statistic between risk groups is based on 1,000 permutations.

of communication within the tumour microenvironment that is necessary for tumour growth and spread. In spite of the overwhelming complexity, modulation of a few key regulatory nodes such as miR-320 may be sufficient to impede the most malignant properties of tumour cells, suggesting strategies for developing agents that disrupt select tumour microenvironment networks. □

METHODS

Methods and any associated references are available in the online version of the paper at http://www.nature.com/naturecellbiology

Note: Supplementary Information is available on the Nature Cell Biology website

ACKNOWLEDGEMENTS

We thank Kara Batte for technical assistance with the microRNA platform, Rumeysa Biyik for bioinformatics assistance, Abdel-Rasoul Mahmoud for statistical assistance and the Ohio State University Human Tissue Resource Network and the Ohio State University Comprehensive Cancer Center Microarray, Nucleic Acids, Proteomic Shared Facilities for technical assistance. This work was funded by grants from the National Institutes of Health to M.C.O. (R01CA053271, P01CA097189) and to G.L. (R01CA85619, R01HD47470, P01CA097189) and from the Komen Breast Cancer Foundation and Evelyn Simmers Charitable Trust to M.C.O.

AUTHOR CONTRIBUTIONS

M.C.O. and G.L. designed and supervised this study, analysed data and helped write and edit the manuscript. A.B. and J.G. designed and carried out experiments, collected and analysed data and co-wrote the paper. J.A.W., H.M., R.S., A.J.T. and F.L. assisted technically with experiments, and collected and analysed data. M.O.N.

assisted with fluorescent and confocal microscopy and immunohistochemistry. L.Y. and S.A.F. contributed to the statistical analyses of data and writing the manuscript. A.S.M., S.C., M.H., M.P. and T.P. contributed to the analysis and comparison of mouse and human profile data. M.G.P. and C.B.M. contributed to the analysis of microRNA data and writing the manuscript. C.K.M., L.D.Y., R.E.J., G.N. and T.J.R. contributed to the histopathological analysis of human samples and writing the manuscript. S.E.L. and E.A.C. contributed to the data analysis and writing the manuscript.

COMPETING FINANCIAL INTERESTS

The authors declare no competing financial interests.

Published online at http://www.nature.com/naturecellbiology
Reprints and permissions information is available online at http://www.nature.com/reprints

1. Mueller, M. M. & Fusenig, N. E. Friends or foes—bipolar effects of the tumour stroma in cancer. *Nat. Rev. Cancer* **4,** 839–849 (2004).
2. Bhowmick, N. A., Neilson, E. G. & Moses, H. L. Stromal fibroblasts in cancer initiation and progression. *Nature* **432,** 332–337 (2004).
3. Kalluri, R. & Zeisberg, M. Fibroblasts in cancer. *Nat. Rev. Cancer* **6,** 392–401 (2006).
4. Eswarakumar, V. P., Lax, I. & Schlessinger, J. Cellular signaling by fibroblast growth factor receptors. *Cytokine Growth Factor Rev.* **16,** 139–149 (2005).
5. Sotgia, F. *et al.* Caveolin-$1^{-/-}$ null mammary stromal fibroblasts share characteristics with human breast cancer-associated fibroblasts. *Am. J. Pathol.* **174,** 746–761 (2009).
6. Trimboli, A. J. *et al.* Pten in stromal fibroblasts suppresses mammary epithelial tumours. *Nature* **461,** 1084–1091 (2009).
7. Di Leva, G. & Croce, C. M. Roles of small RNAs in tumor formation. *Trends Mol. Med.* **16,** 257–267.
8. Ventura, A. & Jacks, T. MicroRNAs and cancer: short RNAs go a long way. *Cell* **136,** 586–591 (2009).
9. Trimboli, A. J. *et al.* Direct evidence for epithelial–mesenchymal transitions in breast cancer. *Cancer Res.* **68,** 937–945 (2008).
10. Bader, A. G., Brown, D. & Winkler, M. The promise of microRNA replacement therapy. *Cancer Res.* **70,** 7027–7030 (2010).
11. Zhang, L. *et al.* microRNAs exhibit high frequency genomic alterations in human cancer. *Proc. Natl Acad. Sci. USA* **103,** 9136–9141 (2006).
12. Ichimi, T. *et al.* Identification of novel microRNA targets based on microRNA signatures in bladder cancer. *Int. J. Cancer* **125,** 345–352 (2009).
13. Schepeler, T. *et al.* Diagnostic and prognostic microRNAs in stage II colon cancer. *Cancer Res.* **68,** 6416–6424 (2008).
14. Mattie, M. D. *et al.* Optimized high-throughput microRNA expression profiling provides novel biomarker assessment of clinical prostate and breast cancer biopsies. *Mol. Cancer* **5,** 24 (2006).
15. Yan, L. X. *et al.* MicroRNA miR-21 overexpression in human breast cancer is associated with advanced clinical stage, lymph node metastasis and patient poor prognosis. *RNA* **14,** 2348–2360 (2008).
16. Borowsky, A. D. *et al.* Syngeneic mouse mammary carcinoma cell lines: two closely related cell lines with divergent metastatic behavior. *Clin. Exp. Metastasis* **22,** 47–59 (2005).
17. Nuovo, G. J. *In situ* detection of precursor and mature microRNAs in paraffin embedded, formalin fixed tissues and cell preparations. *Methods* **44,** 39–46 (2008).
18. Jorgensen, S., Baker, A., Moller, S. & Nielsen, B. S. Robust one-day in situ hybridization protocol for detection of microRNAs in paraffin samples using LNA probes. *Methods* **52,** 375–381 (2010).
19. Nuovo, G., Lee, E. J., Lawler, S., Godlewski, J. & Schmittgen, T. *In situ* detection of mature microRNAs by labeled extension on ultramer templates. *Biotechniques* **46,** 115–126 (2009).
20. Obernosterer, G., Leuschner, P. J., Alenius, M. & Martinez, J. Post-transcriptional regulation of microRNA expression. *RNA* **12,** 1161–1167 (2006).
21. Politz, J. C., Hogan, E. M. & Pederson, T. MicroRNAs with a nucleolar location. *RNA* **15,** 1705–1715 (2009).
22. Kim, D. H., Saetrom, P., Snove, O. Jr & Rossi, J. J. MicroRNA-directed transcriptional gene silencing in mammalian cells. *Proc. Natl Acad. Sci. USA* **105,** 16230–16235 (2008).
23. Huber, M. A., Kraut, N. & Beug, H. Molecular requirements for epithelial–mesenchymal transition during tumor progression. *Curr. Opin. Cell Biol.* **17,** 548–558 (2005).
24. Hanahan, D. & Weinberg, R. A. The hallmarks of cancer. *Cell* **100,** 57–70 (2000).
25. Hughes, C. C. Endothelial–stromal interactions in angiogenesis. *Curr. Opin. Hematol.* **15,** 204–209 (2008).
26. Orlichenko, L. S. & Radisky, D. C. Matrix metalloproteinases stimulate epithelial–mesenchymal transition during tumor development. *Clin. Exp. Metastasis* **25,** 593–600 (2008).
27. Mongiat, M. *et al.* The extracellular matrix glycoprotein elastin microfibril interface located protein 2: a dual role in the tumor microenvironment. *Neoplasia* **12,** 294–304 (2010).
28. Aoyama, T. *et al.* Structure and chromosomal assignment of the human lectin-like oxidized low-density-lipoprotein receptor-1 (LOX-1) gene. *Biochem. J.* **339,** 177–184 (1999).
29. Yan, S., Berquin, I. M., Troen, B. R. & Sloane, B. F. Transcription of human cathepsin B is mediated by Sp1 and Ets family factors in glioma. *DNA Cell Biol.* **19,** 79–91 (2000).
30. Cironi, L. *et al.* IGF1 is a common target gene of Ewing's sarcoma fusion proteins in mesenchymal progenitor cells. *PLoS One* **3,** e2634 (2008).
31. He, H. J., Kole, S, Kwon, Y. K., Crow, M. T. & Bernier, M. Interaction of filamin A with the insulin receptor alters insulin-dependent activation of the mitogen-activated protein kinase pathway. *J. Biol. Chem.* **278,** 27096–27104 (2003).
32. de Kerchove D'Exaerde, A. *et al.* Expression of mutant Ets protein at the neuromuscular synapse causes alterations in morphology and gene expression. *EMBO Rep.* **3,** 1075–1081 (2002).
33. Tomarev, S. I. & Nakaya, N. Olfactomedin domain-containing proteins: possible mechanisms of action and functions in normal development and pathology. *Mol. Neurobiol.* **40,** 122–138 (2009).
34. Hollander, M. C., Blumenthal, G. M. & Dennis, P. A. PTEN loss in the continuum of common cancers, rare syndromes and mouse models. *Nat. Rev. Cancer* **11,** 289–301 (2011).
35. Rong, Y. *et al.* Epidermal growth factor receptor and PTEN modulate tissue factor expression in glioblastoma through JunD/activator protein-1 transcriptional activity. *Cancer Res.* **69,** 2540–2549 (2009).
36. Vivanco, I. *et al.* Identification of the JNK signaling pathway as a functional target of the tumor suppressor PTEN. *Cancer Cell* **11,** 555–569 (2007).
37. Finak, G. *et al.* Stromal gene expression predicts clinical outcome in breast cancer. *Nat. Med.* **14,** 518–527 (2008).
38. Finak, G. *et al.* Gene expression signatures of morphologically normal breast tissue identify basal-like tumors. *Breast Cancer Res.* **8,** R58 (2006).
39. Pawitan, Y. *et al.* Gene expression profiling spares early breast cancer patients from adjuvant therapy: derived and validated in two population-based cohorts. *Breast Cancer Res.* **7,** R953–R964 (2005).

DOI: 10.1038/ncb2396

METHODS

Cell culture. Primary *Pten*$^{+/+}$ or *Pten*$^{-/-}$ MMFs were purified as previously described[6]. *Pten*$^{-/-}$ MMFs were immortalized using a 3T3 protocol[40]. MMFs, DB7 (16) and COS7 cells were cultured in DMEM containing 10% fetal bovine serum under standard conditions. Endothelial cells were cultured in DMEM-F12 containing 20% fetal bovine serum plus 30 μg ml^{-1} endothelial-cell growth supplement (Upstate Biotechnology) and 10 U ml^{-1} heparin (Sigma-Aldrich).

miR profiling and quantitative PCR. Total RNA was extracted using Trizol (Invitrogen) and treated with RNase-free DNase (Qiagen). MicroRNA profiling was carried out as described previously[41]. Mature miR expression analysis by qrtPCR was carried out using the miR real-time PCR detection kit (Applied Biosystems) as described previously[42]. Quantitative real-time PCR expression analysis with reverse transcription was carried out using Power SYBR Green (Applied Biosystems) with mouse *Ets2*, *Mmp9* and 18S ribosomal RNA primers. Primer sequences (5′-3′) were: *Mmp9*, 5′-cattcgcgtggataaggagt-3′ and 5′-tcacacgccagaagaatttg-3′; *Ets2*, 5′-ccaaaaggagcaacgacgtct-3′ and 5′-ttcatgccaaactggtgcag-3′; 18S rRNA, 5′-aactttcgatggtagtcgccg-3′ and 5′-ccttggatgtggtagccgttt-3′.

Microarray analysis. Fibroblasts and epithelial cells were isolated from mammary glands of wild-type mice or mice with *Pten*-null fibroblasts by methods described previously[6]. Endothelial cells in collagenase-dispersed tissue from these same mammary glands were labelled with CD31 fluorescently tagged antibody (BD Pharminogen) and enriched using fluorescence-activated cell sorting. RNA was collected with Trizol (Invitrogen). RNA samples were hybridized to Affymetrix Mouse Exon 1.0 ST Array platform. Data were processed using Affymetrix Expression Console software. The Robust Multichip Average method was used to do background correction, quantile normalization, and expression level summarization. For each cell compartment, twofold differentially expressed genes at a significance level of $P < 0.05$ were determined by using BRB-Array Tools 3.8.1. For construction of heat maps, the geometric means of genes from wild-type samples in each cell compartment are set as references, and the colours (from blue to red) represent the ratio between the gene expression in samples and the references. Global gene-expression data from the three cell compartments was also analysed by principal component analysis using the Statistical R package. The first three principal components explained the largest variation of gene-expression differences.

The microarray data were deposited with Gene Expression Omnibus and can be viewed at http://www.ncbi.nlm.nih.gov/geo/query/acc.cgi?token=dncnfwwoqoqyexc&acc=GSE24501.

Vector construction and transfection. The lentiviral pMIR–GFP, pMIR–GFP-containing *miR-320* precursor RNA, pCMV-SPORT6 *Ets2* full-length and pCMV-SPORT6 *Mmp9* full-length vectors were purchased from Open BioSystem, and pCMV6 *Emilin2* full-length vector was purchased from OriGene.

The 3′UTRs encompassing the target sequence for miR-320 of *Ets2* and *Mmp9* cDNAs were cloned into the pMIR-REPORT vector (Ambion). Luciferase reporter vector pEZX-MT01 containing the full-length 3′UTR of the *Emilin2* gene was purchased from GeneCopoeia. Luciferase reporter assays were carried out as previously described[43]. For the mutated construct of pCMV-SPORT6 *Ets2* the QuickChange Site-Directed Mutagenesis Kit (Stratagene) was used to alter the miR-320 seed sequence. Transfection (25–75 nmol l^{-1}) of scrambled miR, pre-miR-320 and anti-miR-320 (Ambion) or pMIR-REPORT was done with Lipofectamine 2000 (Invitrogen).

The pMIR-lentiviral constructs along with lentiviral packaging constructs (System Biosciences) were used to establish *Pten*$^{-/-}$ MMF lines constitutively overexpressing GFP or GFP–miR-320 (Supplementary Fig. S3c).

siRNA for *Mmp9* (5′-CTGGAAGGTATTATGTAACTA-3′), *Emilin2* (5′-AGGCGTTGTTCTCTTCAATAA-3′), *Akt1* (5′-CATGCTGTTCAGAGACATTTA-3′), *Mapk8* (5′-ATGAAGTGTGTTAATCACAAA-3′) and *Mapk9* (5′-ACCGTCAT-ATATCATATCTTA-3′) were purchased from QIAGEN.

Xenograft assays. All use of animals was in accordance with all US National Institutes of Health regulations and were approved by the Ohio State University Institutional Animal Care and Use Committee. Female NcR nude mice were purchased from Taconic. For cell co-injections, 1.5×10^6 DB7 cells (stably transfected with pDSRed2-C) and 0.5×10^6 MMFs (infected or transfected, as shown in figure legends) were suspended in a 0.2 ml mixture of serum-free DMEM and ice-cold Matrigel (BD Biosciences) at a 1:1 ratio and injected subcutaneously. Each nude mouse was injected at two sites, one each for control and experimental admixtures (see figure legends). For tumour formation assays mice were killed 4 weeks after injection; for angiogenesis and BrdU incorporation analyses mice were killed 5 days after cell injections. Tumours (4 weeks) or Matrigel composites (5 days) were collected, weighed and either fixed immediately in 10% formalin and embedded in paraffin, or frozen in OCT. Histological sections 30 μm in thickness were prepared for evaluation of RFP and GFP expression, or CD31 (1:40 antibody dilution) and BrdU immunostaining. Confocal microscopy was carried out as previously described[44].

ISH and IHC of human TMAs. TMAs were constructed from de-identified invasive breast carcinoma patient samples ($n = 126$). The TMAs consisted of three cores for each tumour sample shown along with three cores of adjacent normal tissue from the same patient. If the adjacent normal samples lacked staining for either miR-320 ISH or PTEN IHC, the samples were excluded from the final analysis (see below). The protocol for detection of miRs by ISH has been previously published[17]. The sequences of the probes (Exiqon) containing the locked nucleic acid/digoxigenin-modified bases were as follows: hsa-miR-320, tcgccctctcaacccagctttt; miR-SC, cgtataggcccaagaattagg. IHC staining for PTEN (1:200) and pT72–ETS2 (anti-peptide rabbit polyclonal 1:40) was carried out as previously described[6]. The Nuance System was used for visualization of ISH and IHC staining as previously described[43].

Preparation of conditioned media and three-dimensional assays. MMFs were cultured until 90% confluent; cells were rinsed twice with serum-free medium, and subsequently incubated in serum-free DMEM for 36 h. The conditioned media were collected and used for *in vitro* assays or for proteomic analysis.

A previously described spheroid migration assay was adapted to mammary tumour cells[44]. Briefly, 8,000 DB7 cells in a 20 μl drop of medium formed mammospheres after 4 days of incubation. The mammospheres were sandwiched between two layers of collagen I in the presence of conditioned medium and quantified as previously described[44].

The vessel-forming ability of endothelial cells was characterized *in vitro* using a Matrigel sandwich assay as previously described[45,46]. ImageJ software (http://rsb.info.nih.gov/ij) was used for quantification of endothelial-cell recruitment into branched networks *in vivo* and *in vitro* using the Analyse Skeleton plugin and Analyse Particles function of binary images with automatic threshold.

BrdU incorporation assay. Cell proliferation was measured using a commercial BrdU assay kit (Roche) following the manufacturer's instructions. BrdU incorporation assays for *in vivo* studies were carried out as previously described[47]. Image J software using the Cell Counter plugin was used to quantify the results.

Proteomic analysis. All mass spectra were acquired at the Proteomics Shared Resource at The Ohio State University. Samples were subjected to nano-liquid chromatography/tandem mass spectrometry to provide internal sequences of the proteins present. Sequence information from the tandem mass spectrometry data was processed using MASCOT 2.0 (Matrix Science). Cell-protein extraction and Western blot analysis was done as described previously[48]. Antibodies used were as follows: LOXL2, MMP2, EMILIN2 (1:500, Santa Cruz Biotechnology), THBS1, THBS2, SFRP1 (1:1,000, R&D Systems), ETS2 (1:1,000, rabbit polyclonal affinity purified), MMP9 (1:1,000, Abcam), BMP1 (1:500, Oncogene), β-actin, α-tubulin (1:10,000, Sigma Aldrich), CTSB, PTEN, AKT, P-AKT^{S473}, JNK, P-JNK$^{T183/Y185}$, ERK and P-ERK$^{T202/Y204}$ (1:1,000, Cell Signaling).

Statistical analysis. For tumour studies (Fig. 1c), an analysis-of-variance model with adjusted pairwise comparisons was used: *Pten*$^{+/+}$ versus *Pten*$^{-/-}$ ($n = 7$) and *Pten*$^{-/-}$ versus *Pten*$^{-/-}$/miR-320 ($n = 9$). Holm's method was used to control false positives[49].

For human TMA studies (Fig. 2a), a nonparametric sign test was used to test paired scores between normal and cancer samples. For dual staining of human TMAs, the Spearman correlation method was used to evaluate the association of scores (Fig. 2a and Supplementary Fig. S2a).

A two-sample Student *t*-test was used for migration, proliferation and angiogenic assays (Figs 1d,e, 3a–d, 4b–e and Supplementary Figs S1d–e).

Generating human stroma heat maps with genes identified from analysis of the miR-320/*Pten*-null MMFs. Genes corresponding to the 54-factor whole secretome identified and the subset of 20 ETS2 targets were queried against the McGill Cancer Center's microarray data on normal and tumour stroma of breast cancer patients (GSE4823; ref. 38). 40 of the 54 genes, and 13 of the 20 ETS2-target genes, were represented on the Custom Agilent Array used in the McGill study[37]. For each of these two gene lists, a heat map was generated on the human stroma dataset (52 normal stroma and 49 tumour stroma samples). The heat maps show the ability of the two gene sets to separate the normal and tumour stroma samples based solely on their gene-expression profiles. The permutation test strategy (10,000 random permutations) was used to confirm that the gene signatures specifically discriminate between human tumour and normal stroma samples.

Kaplan–Meier curves for survival risk prediction using principal component analysis with genes identified from analysis of the miR-320/*Pten*-null mouse fibroblasts. All analyses were carried out using BRB-Array Tools. The Survival Risk Group Prediction Tool was used to analyse whether the

miR-320/*Pten*-related 54-gene signature (40 human orthologues) and the 20 ETS2-target genes (13 human orthologues) have a statistically significant association with the survival data for patients within each dataset. This regression model enables the analysis of survival risk for each individual as a function of the logged gene-expression values. The subset of genes that correlated with time through a univariate analysis was obtained using a Cox threshold significance level of 0.05. The evaluation of the predictive method was cross-validated using the tenfold cross-validation. The statistical significance for the survival curves was found by calculating the log-rank statistical P value by carrying out 1000 permutations. All other parameters were set to the default values. The McGill stromal database (GSE4823, Fig. 6b,d) and the Stockholm whole-tumour database (GSE1456 Supplementary Fig. S5a,b) were used for the analyses.

40. Todaro, G. J. & Green, H. Quantitative studies of the growth of mouse embryo cells in culture and their development into established lines. *J. Cell Biol.* **17,** 299–313 (1963).
41. Hunter, M. P. *et al.* Detection of microRNA expression in human peripheral blood microvesicles. *PLoS One* **3,** e3694 (2008).
42. Godlewski, J. *et al.* Targeting of the Bmi-1 oncogene/stem cell renewal factor by microRNA-128 inhibits glioma proliferation and self-renewal. *Cancer Res.* **68,** 9125–9130 (2008).
43. Godlewski, J. *et al.* MicroRNA-451 regulates LKB1/AMPK signaling and allows adaptation to metabolic stress in glioma cells. *Mol. Cell* **37,** 620–632 (2010).
44. Nowicki, M. O. *et al.* Lithium inhibits invasion of glioma cells; possible involvement of glycogen synthase kinase-3. *Neuro. Oncol.* **10,** 690–699 (2008).
45. Rothhammer, T., Bataille, F., Spruss, T., Eissner, G. & Bosserhoff, A. K. Functional implication of BMP4 expression on angiogenesis in malignant melanoma. *Oncogene* **26,** 4158–4170 (2007).
46. Srinivasan, R. *et al.* Erk1 and Erk2 regulate endothelial cell proliferation and migration during mouse embryonic angiogenesis. *PLoS One* **4,** e8283 (2009).
47. Chong, J. L. *et al.* E2f1–3 switch from activators in progenitor cells to repressors in differentiating cells. *Nature* **462,** 930–934 (2009).
48. Bronisz, A. *et al.* Microphthalmia-associated transcription factor interactions with 14-3-3 modulate differentiation of committed myeloid precursors. *Mol. Biol. Cell* **17,** 3897–3906 (2006).
49. Holm, S. A simple sequentially rejective multiple test procedure. *Scand. J. Stat.* **6,** 65–70 (1979).

nature cell biology

DOI: 10.1038/ncb2396

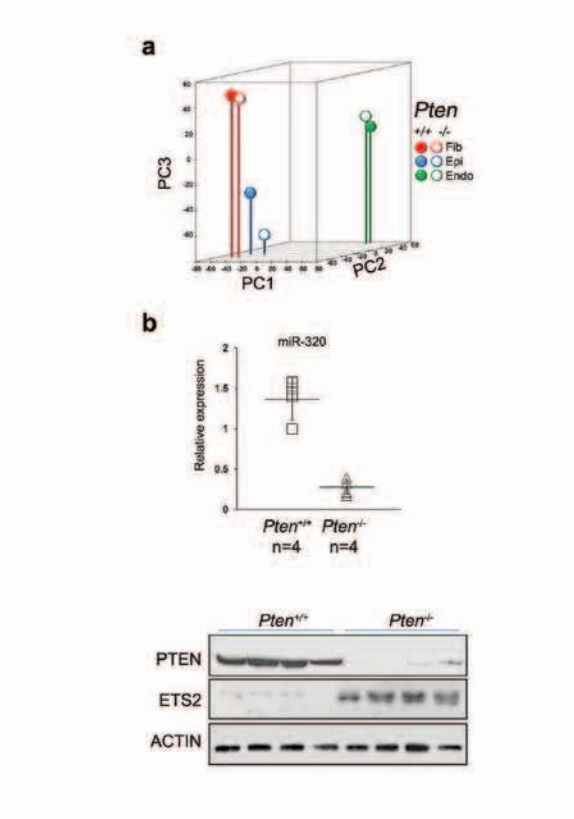

Figure S1 Global analysis of mRNA expression in Pten$^{+/+}$ and Pten$^{-/-}$ primary MMFs by Principal Component Analysis. **a.** Gene profiling was performed (n=2) on epithelial (Epi) and endothelial cells (Endo) from mammary glands with *Pten*$^{+/+}$ or *Pten*$^{-/-}$ MMFs (Fib), as indicated. Principal component analysis (PCA) was performed to visualize gene expression results from these samples; results are shown in 3-dimensions (right panel). The PCA analysis confirm that Pten status in fibroblasts affects gene expression in the epithelial and endothelial cell compartments. miR320 expression correlates directly with PTEN and inversely with ETS2 expression in *Pten*$^{+/+}$ and *Pten*$^{-/-}$ primary MMFs. Expression of miR-320 was measured by qRT-PCR in *Pten*$^{+/+}$ or *Pten*$^{-/-}$ MMFs (upper graph). Values are expressed as mean relative miR-320 expression level ±SD, p-value = 0.0008. Cell lysates from *Pten*$^{+/+}$ (n=4) or *Pten*$^{-/-}$ (n=4) MMFs, paired with RNA samples from Figure S1a, were blotted with anti-PTEN or anti-ETS2 antibody and anti-β-actin antibody as a loading control (bottom panel).

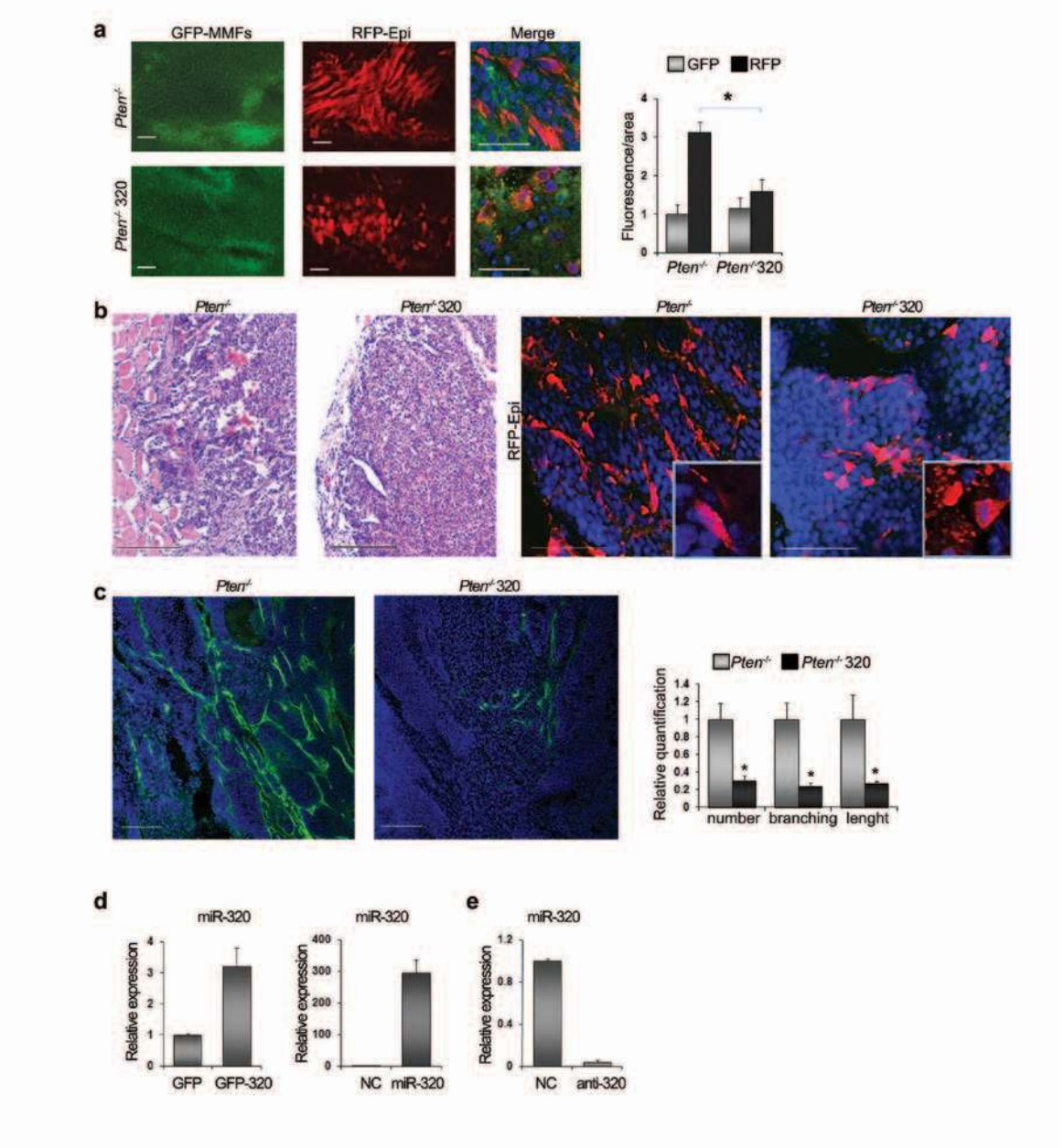

Figure S2 Difference in tumor weights formed by DB7 cells combined with *Pten*$^{-/-}$ or *Pten*$^{-/-}$ miR-320 MMFs are the result of increased growth of the epithelial tumor cells *in vivo*. *Pten*$^{-/-}$ or *Pten*$^{-/-}$ miR-320 MMFs tagged with eGFP were admixed with ds-Red-tagged DB7 cells and grown for four weeks subcutaneously in athymic mice. Importantly, injection of MMFs alone, regardless of genotype, never resulted in tumors (not shown). Representative confocal microscope images of DB7 cells (RFP-positive) and *Pten*$^{-/-}$ or *Pten*$^{-/-}$ miR-320 MMFs (GFP-positive) in 30 μM sections prepared from frozen tumors grown subcutaneously in athymic mice. Green (GFP, left panels), red (RFP, middle panels) and merged (RFP/GFP/ and blue DAPI, right panels) channels are shown. Scale bars: 25μm. Data was quantified using Image J (graph on the right) using total fluorescence signal of both types from 6 random images from each of three different tumor pairs. Data expressed as mean ±SD $^{*}p = 0.0017$. Tumors formed by DB7 cells with Pten$^{-/-}$ or Pten$^{-/-}$ miR-320 MMFs have different invasive phenotypes *in vivo*. *Pten*$^{-/-}$ or *Pten*$^{-/-}$ miR-320 MMFs were admixed with DB7 cells and grown for four weeks subcutaneously in athymic mice. Representative micrographs of thin H&E stained sections from fixed, paraffin imbedded tumors are shown (two left panels). Scale bars: 200μm. Representative confocal microscope images of DB7 cells (RFP-positive) in 30 μm frozen sections as above are shown as merged red (RFP) and blue (DAPI) channels (two right panels). Scale bars: 50μm. The inserts are magnified x2.5. Note that these confocal images also revealed the infiltration of host stromal cells, recognized by DAPI staining, into tumors derived from every fibroblast-epithelial cell combination.Tumors formed by DB7 cells with *Pten*$^{-/-}$ or *Pten*$^{-/-}$ miR-320 MMFs have different levels of tumor blood vessel formation *in vivo*. *Pten*$^{-/-}$ or *Pten*$^{-/-}$ miR-320 MMFs were admixed with DB7 cells and grown for four weeks subcutaneously in athymic mice. Representative microscope images of paraffin imbedded tissue with blood vessels visualized by indirect immunofluorescent staining of the endothelial marker CD31 (merged image, CD-31 – green, DAPI - blue). Scale bars: 50μm. n=18 images taken form 3 different mice. Data expressed as mean ±SD $^{*}p < 0.01$. Increased miR-320 expression in Pten-/- MMFs following GFP-miR-320 lentiviral transduction or transfection of miR-320 oligonucleotides. Expression of miR-320 was validated by qRT-PCR (n=3). Values are expressed as mean relative miR expression level ±SD. , Expression of free miR-320 in Pten+/+ MMFs is lowered by transfection of anti-miR-320 oligonucleotide. Expression of miR-320 was validated by qRT-PCR (n=3). Values are expressed as mean relative miR expression level ±SD.

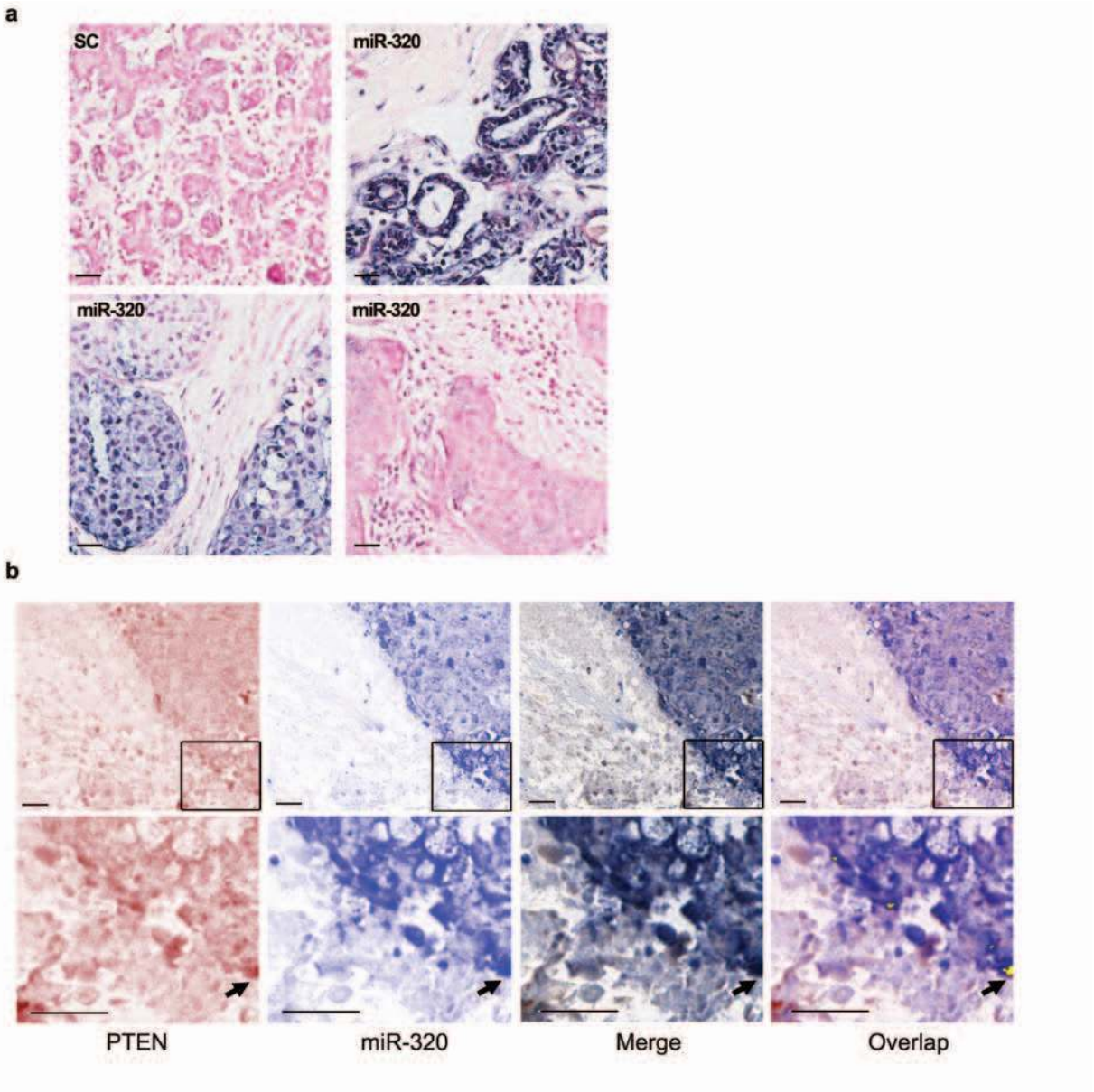

Figure S3 MiR-320 is downregulated in breast cancer stroma. Representative images of miR-320 ISH staining (blue) with eosin counterstain (pink) in human normal (control) and cancer breast tissue; scrambled control was performed on adjacent normal breast tissue. Scale bars: 50μm. Images were captured using the light microscope. Coordinate loss of MiR-320 and *PTEN* in undifferentiated invasive breast cancer. Representative images of a human breast carcinoma sample that has low stromal expression of both miR-320 (detected by ISH) and *PTEN* (detected by IHC). Images made with the Nuance multifocal system as in Fig 2. Upper panels - low magnification; bottom panels - high magnification. Scale bars: 50μm**.** The inserts are magnified x3. Co-localized staining of both markers was converted to fluorescence yellow signal, and the small area of co-localization in the tumor is indicated by the arrow.

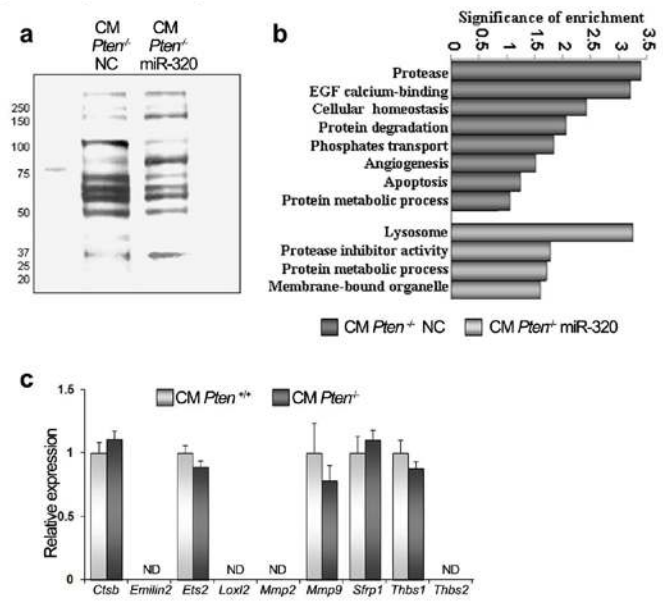

Figure S4 Expression of miR-320 in Pten-/- MMFS alters the pattern of secreted proteins. Coomassie staining of 30x concentrated conditioned medium (CM) from *Pten*$^{-/-}$MMFs transfected with either miR negative control (NC) or miR-320 precursors (miR-320), as indicated. Expression of miR-320 in Pten-/- MMFs alters the composition of the secretome. Proteins identified by mass-spectrometry as specific to either MMFs *Pten*$^{-/-}$ NC or *Pten*$^{-/-}$ 320 were analyzed by DAVID Functional Annotation Tool (http://david.abcc.ncifcrf.gov/). Major GO categories enriched are depicted. Conditioned media from MMFs *Pten*$^{+/+}$ or *Pten*$^{-/-}$ do not alter expression of the miR-320 targets in DB7 cells. DB7 cells were treated with conditioned medium (CM) from either *Pten*$^{+/+}$ or *Pten*$^{-/-}$ MMFs. Expression of selected miR-320/ETS2 targets was validated by qRT-PCR (n=3). Values are expressed as mean relative gene expression level ±SD, ND (not detectable).

a

	predicted consequential pairing of target region	
1116 : 5′	UGUAAUUUGUAAGAAAGCUUUA	*Ets2*
	AGCGGGAGAGUUGGGUCGAAAA	mmu-miR-320
	UGUAAUUUGUAAGAAAGCGGGA	*Ets2 mut*
375 : 5′	GGGCUCUCUCUGCCCACCGUCC	*Mmp9*
3′	AGCGGGAGAGUUGGGUCGAAAA	mmu-miR-320
39 : 5′	GUGAAAACUCCAA--AGCUUUAA	*Emilin2*
3′	AGCGGGAGAGUUGGGUCGAAAA	mmu-miR-320

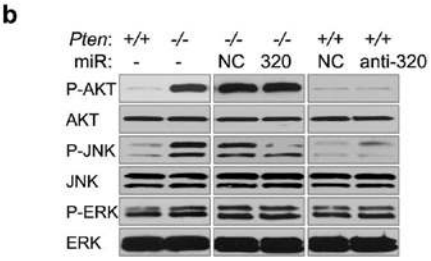

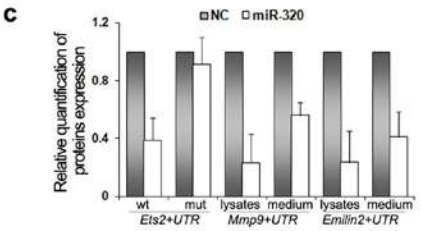

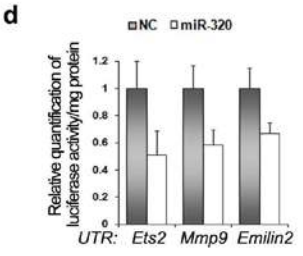

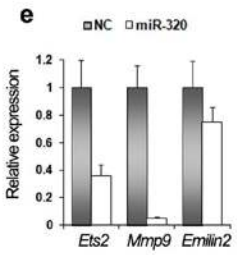

Figure S5 Sequences of *Ets2, Mmp9* and *Emilin2* 3'UTRs. Sequences of wt miR-320 target site within murine *Ets2, Mmp9* and *Emilin2* 3'UTRs, respectively. The mutation targeting the miR-320 seed sequence in *Ets2* 3' UTR is depicted (GGGA replacing UUUA). Effect of miR-320 on PTEN downstream signaling. *Pten*$^{+/+}$ and *Pten*$^{-/-}$ MMFs were left untreated (lane 1 and 2) or were transiently transfected with miR negative control (NC), miR-320 precursors (320) or anti-miR-320 (anti-320), respectively. Whole cell lysates were blotted with anti-AKT, JNK and ERK antibodies recognizing both phospho- (P) and total protein. Densitometric evaluation of protein expression. COS7 cells were transfected (n=4) with full length cDNA (5'-UTR/ORF/3'-UTR) of: *Ets2* (*Ets2*+UTR) wild type (wt) or mutated in miR-320 seeding region (mut) expression vector, *Mmp9* (*Mmp9*+UTR) or *Emilin2* (*Emilin2*+UTR) and co-transfected with either miR negative control (NC) or miR-320 precursors (320). Western blotting shown on Figures 5b, c were quantified by densitometric analysis using ImageJ software, normalized to loading control. Mean relative expression level ±SD is shown. Direct targeting of *Ets2* 3 UTR, *Mmp9* 3 UTR and *Emilin2* 3'UTR by miR-320 in luciferase reporter constructs. COS7 cells were transfected (n=3 experiments, each performed in triplicate) with a luciferase reporter vector containing the *Ets2, Mmp9* or *Emilin2* 3'UTRs, and co-transfected with either miR negative control (NC) or pre-miR-320 (320). Luciferase levels are expressed as mean relative to controls ±SD. Effect of miR-320 on *Ets2, Mmp9* and *Emilin2* mRNA levels. Cells were transiently transfected with either miR negative control (NC) or pre-miR-320 (miR-320). *Ets2*, *Mmp9* and *Emilin2* mRNA levels were measured by qRT-PCR (n=3) and expressed as mean ±SD.

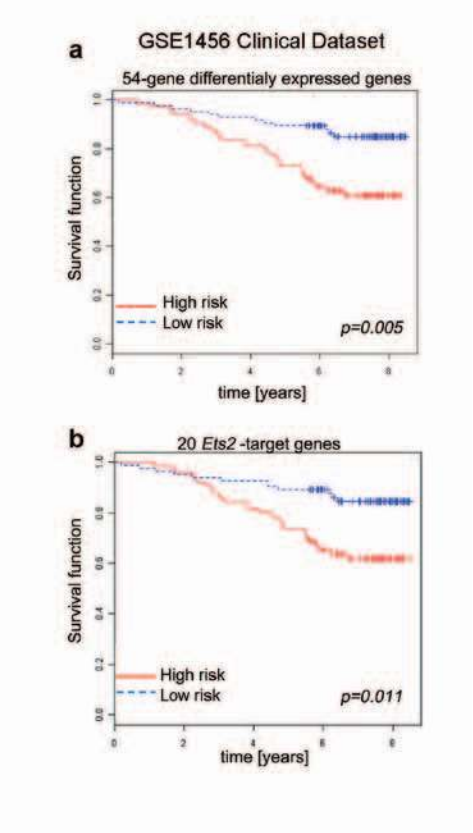

Figure S6 The miR-320 secretome gene expression signature correlates with breast cancer patient outcome. Kaplan-Meier curves of patient outcomes segregated by expression of the "secretome genes". The 159-patient Stockholm microarray data set (GSE1456) that contained gene expression profiles from whole tumors was used; 48 of 54 secretome genes were retrieved in this data base. The permutation p-value of the log-rank test statistic between risk groups is based on 1000 permutations. The Ets2 secretome signature correlates with breast cancer patient outcomes expression profiles. Kaplan-Meier curves using the ETS2-regulated secretome, as above. The GSE1456 microarray contained 17/20 of the Ets-2 targets. The permutation p-value of the log-rank test statistic between risk groups is based on 1000 permutations.

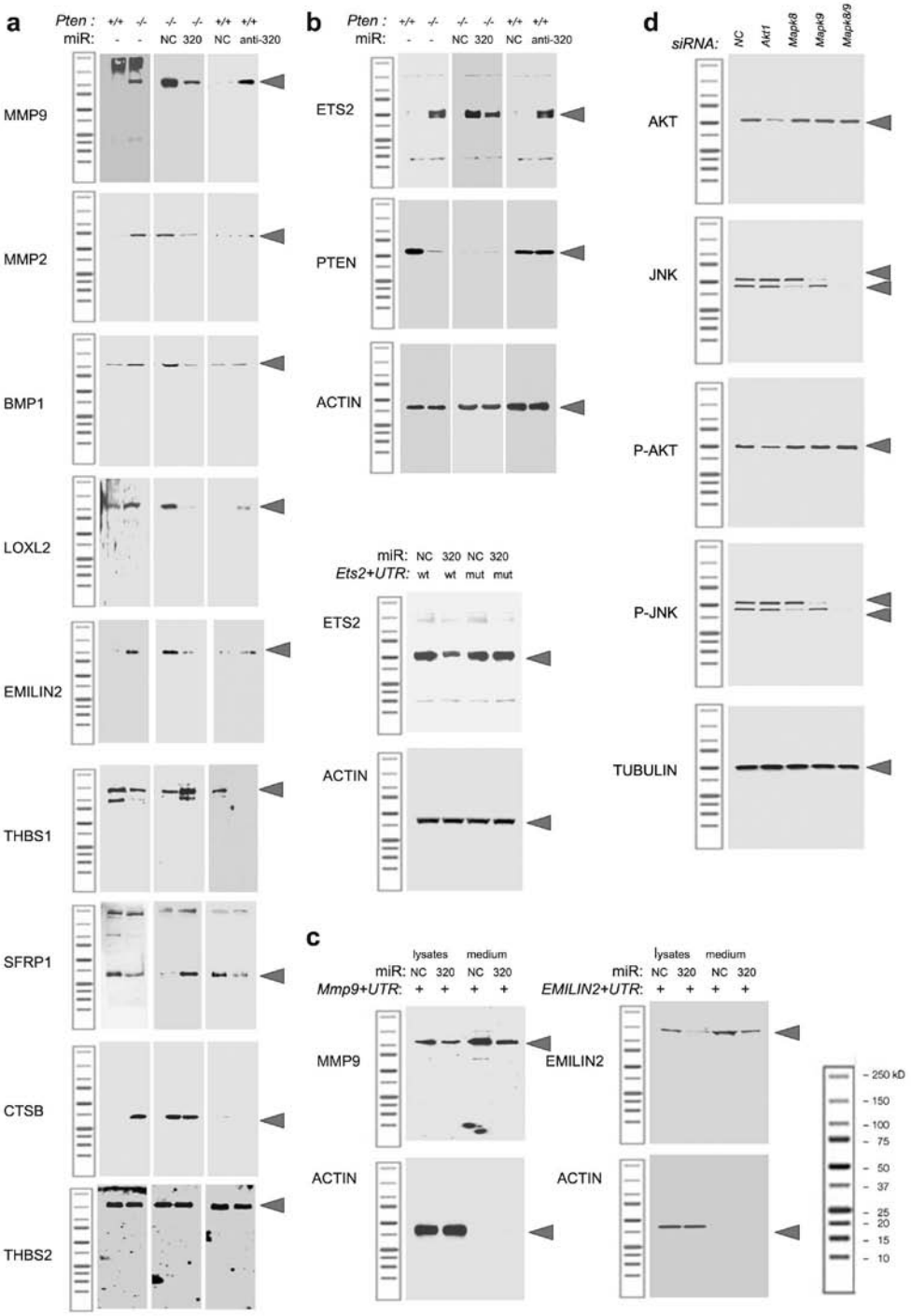

Figure S7 Full length blots from Fig. 4a. Full length blots from Fig. 5ab. Full length blots from Fig. 5c. Full length blots from Fig. 5d

Supplementary Tables

Table S1 List of microRNAs down regulated in *Pten*$^{-/-}$ MMFs (>2.5-fold and p<0.05)

Table S2 Spearman correlations between *PTEN*, P-ETS2^{T72} and miR-320 expression in stroma and/or epithelium based on Allred scores of the tissue microarray (See Methods).

Table S3 List of secreted proteins identified by mass spectrometry in conditioned medium from *Pten*$^{-/-}$ MMFs transfected with either miR negative control (NC) or miR-320 precursor. Mir-320 targets, predicted *in silico* (www.microran.org; www.targetscan.org) are indicated in red.

Table S4 List of secreted proteins identified by mass spectrometry in conditioned medium from *Pten*$^{-/-}$ MMFs with conserved ETS2 binding sites in 5' non-coding region.

Table S5 List of 40 differentially expressed genes shown on the heatmap on Figure 6A and list of 13 Ets2-target genes shown on the heatmap on Figure 6c (in order of appearance).